Feasibility of Direct Air to Ground Communication via a Terrestrial 5G Network

Syed Aizaz Ali Shah*, Thomas Meyerhoff†, Rainer Grünheid*, Gerhard Bauch* and Dominic Schupke†
*Institute of Communications, Hamburg University of Technology, Hamburg, Germany.
†Central Research and Technology, Airbus Operations GmbH, Hamburg/Munich, Germany.
Email: aizaz.shah@tuhh.de, thomas.meyerhoff@airbus.com, {gruenheid, bauch}@tuhh.de, dominic.schupke@airbus.com

***Abstract*—This feasibility study deals with Air to Ground (ATG) communications between a 5G type Terrestrial Mobile Communication Network (TMCN) and an User Equipment (UE) installed onboard a passenger aircraft in approach to an airport. The network model is based on real gNodeB (gNB) deployment data and optimized for serving terrestrial UEs. The evaluation concerns a scenario in which the passenger aircraft is supported by a remote operator via an ATG link to assist its safe landing. To mitigate the interference expected to arise in ATG communications, the aircraft is assumed to be equipped with an Active Electronically Scanned Array (AESA). The simulation results discussed in this paper address the Signal to Interference power Ratio (SIR), link availability, and handover process during ATG communications along representative approach trajectories for different AESA configurations and levels of support by the TMCN. It is shown that SIR above $30\,$dB and link availability upto 97.7% can be achieved by using an 8×8 AESA at the aircraft when the network provides support in the form of dedicated radio resources. It is observed that the frequency of handovers increases with improving link quality.**

I. Introduction

In aviation, the concept of remote operation is typically associated with Uncrewed Aerial Vehicles (UAVs). However, it may also be applied to passenger aircraft in the future. One possible use case could be to improve flight safety by enabling a remote operator to assist the landing of an aircraft e.g. in an emergency. In this case, wireless transmission of Command and Control (C2) information between an aircraft and the remote operator will be required. Consequently, the C2 link will be subjected to strict availability, reliability and latency requirements [1].

The ubiquity of TMCNs such as LTE and 5G and their infrastructure make these networks promising candidates for connecting a remote operator to an aircraft. In that context, an UE onboard aerial vehicles is referred to as Aerial User Equipment (aUE) and the communication between an aUE and a TMCN is referred to as ATG communications.

ATG communications have been studied intensively in the context of beyond line of sight communications for UAVs flying at low altitudes. Field test and simulation results for aUE moving over LTE networks at a height of up to $300\,$m are discussed in [2]–[6]. The results, e.g., in [6], indicate that the downlink quality should be sufficient for C2 links at altitudes up to $120\,$m. ATG communications between UAVs and 5G networks is also explored, for example, in [7]–[9]. The support of aUEs onboard UAVs by 5G networks is already a part of the standardization [10].

Cellular connectivity for high altitude aUEs, such as aircraft, is also of interest. The European Aviation Network (EAN) is an ATG communication system that is offering seamless in-flight broadband connectivity for commercial passenger aircraft via satellites and dedicated, sparsely deployed LTE Base Stations (BSs) with mechanically up-tilted antennas covering the airspace [11]. Efforts to provide broadband connectivity to passengers onboard aircraft via 5G networks are already underway [12].

ATG communication with an aUE is subject to strong interference in both up- and downlink [2]–[9]. Network based solutions to mitigate the interference include partitioning of the radio resources between terrestrial and aUEs, inter-cell interference coordination methods and power control mechanisms [4], [6], [13], [14]. The use of directional antennas on UAVs has been identified as a key aUE based solution to combat interference [2], [14]–[18]. The use of an AESA onboard an UAV that is capable of tracking a serving BS with its beam can significantly reduce the rate of handovers and probability of communication outage [18].

Contrary to the EAN and 5G related ATG standardization activities for high altitude aUEs [12], this work concerns ATG communications for C2 links. We assume a case of emergency requiring safe landing of the aircraft at the nearest airport, which must be supported by the remote operator. The results presented hereafter give a first reference to the feasibility of using an existing TMCN in this context and illustrate the challenges arising from the use of infrastructure optimized for terrestrial coverage.

II. Air to Ground Communication Model

The ATG communication model considered in this study is depicted in Fig. 1 and consists of:

- a 5G TMCN with gNBs equipped with down-tilted sector antennas, i.e., primarily intended for terrestrial users,
- an aUE installed at an aircraft on approach trajectory,
- terrestrial UEs and
- a Ground Operations Center (GOC) that is facilitating a remote operator with a wired communication link to the TMCN.

The authors would like to thank Stefan Neumann (Hamburg University of Technology) for assisting with the simulations.

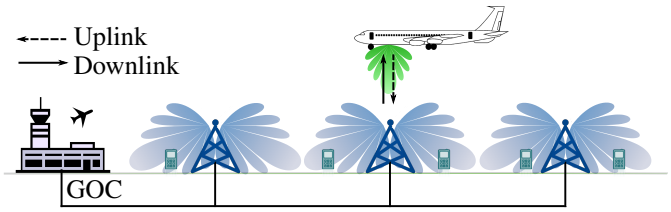

Fig. 1. ATG communications towards an aircraft in approach

The aUE communicates with a serving gNB on up- and downlink. The serving gNB relays the data to the GOC through a wired backhaul. The remote operator is located in the GOC and able to control the aircraft via a C2 link. In this regard, it is expected that an aUE onboard an aircraft in approach:

- is in radio range to many gNBs,
- is predominantly served via the side lobes of the down-tilted sector antennas,
- experiences severe interference on the downlink and
- causes interference on the uplink of terrestrial UEs.

Similar to the case of UAVs, the challenges for ATG communication with an aircraft in approach are to maintain a sufficient link budget towards the serving gNB and mitigate interference. However, for the latter, the interference effects are expected to be more severe compared to the case of UAVs, as there will be significantly more gNBs in radio range due to the high altitude of the aUE.

In this work, the feasibility of ATG communications for aircraft in approach is studied with simulations on link budget level. The study focuses on the downlink only because the anticipated strong interference poses a greater challenge for an aUE as compared to terrestrial UEs. It is assumed that interference caused by an aUE in an emergency situation is tolerated.

The simulation is based on the following model blocks:

A. Terrestrial Mobile Communication Network

The terrestrial network model is composed of gNBs with high transmit power levels, low operating frequencies and high antenna masts. These properties can be considered as advantageous for ATG communications and are typical for gNBs intended for rural coverage.

To create the network model, real deployment information of gNBs in the vicinity of the Zurich international airport was obtained from the data provided by [19]. The data set contains the gNB locations and their classification into four categories based on their total radiated powers. Therefore, the network model was created from the data set in two steps: First, only the gNBs that belong to the category of highest total radiated power are considered. Second, inspired from the description of rural macro scenario in [20], a minimum Inter-site Distance (ISD) of $1,732\,\mathrm{m}$ is enforced since a mobile operator will not install these type of gNBs very close to each other. The resulting network comprised by the set $\mathcal{G}_{\mathrm{Sw}}$ of gNBs is depicted in Fig. 2 by the grey dots.

Due to close proximity of the Zurich airport to international borders, it is vital to consider the presence of 5G networks

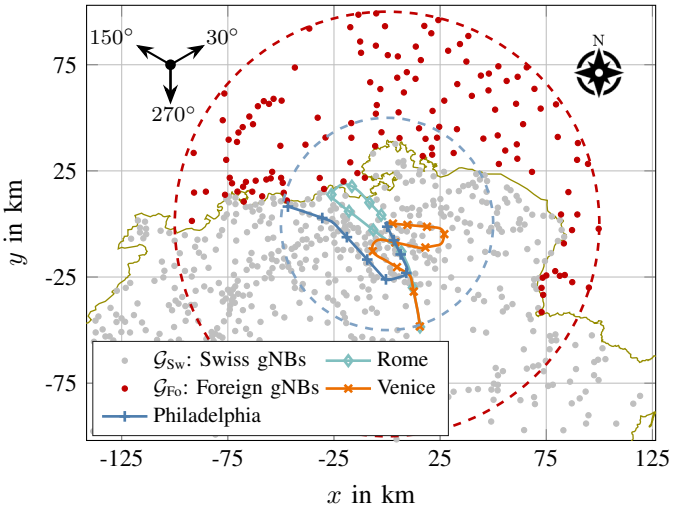

Fig. 2. 5G network for rural coverage in Switzerland along with foreign 5G network in neighboring countries within 100 km of Zurich airport.

in the neighboring countries. A foreign rural 5G network composed of a set $\mathcal{G}_{\mathrm{Fo}}$ of gNBs is considered within $100\,\mathrm{km}$ radius of Zurich airport, depicted by red dots in Fig. 2. The deployment of the foreign gNBs is estimated, based on public data of 5G coverage in the neighboring countries[1]. To facilitate ATG communications during the complete approach, a coverage area of $50\,\mathrm{km}$ radius around the Zurich airport (blue circle in Fig. 2) is considered.

B. Aerial User Equipment and gNodeB

The aUE is installed onboard a passenger aircraft and connected to a square AESA. The AESA is integrated into the underside of the fuselage with its boresight pointed downwards, as indicated in Fig. 1. The antenna array consists of N_{e} elements, spaced at 0.5λ, in both horizontal and vertical directions where λ is the carrier wavelength in meters. The individual array elements are modeled according to [20]. Further, the aircraft orientation is constrained such that its roll and pitch axis remain parallel to the earth surface during its flight.

Each gNB is modeled with a mast height of $h_{\mathrm{gNB}}{=}35\,\mathrm{m}$ and three sector antennas pointed towards $30°, 150°$ and $270°$ azimuth (top left of Fig. 2). Each sector antenna is a fixed beam $8{\times}1$ vertical Uniform Linear Array (ULA) with 0.5λ element spacing and has a mechanical down-tilt of $3°$ [21]. The array elements are modeled according to [20]. A transmit power of $46\,\mathrm{dBm}$ is assumed for each cell. Relevant parameters of the gNB and aUE models are summarized in Table I.

C. Link Budget

The average received power observed by the aUE from any gNB sector is computed as:

$$\bar{P}_{\mathrm{R,dBm}} = P_{\mathrm{T,dBm}} + G_{\mathrm{T,dBi}} + G_{\mathrm{R,dBi}} - L_{\mathrm{dB}}, \qquad (1)$$

[1]https://www.telekom.de/netz/mobilfunk-netzausbau, https://www.magenta.at/unternehmen/netz and https://www.nperf.com/en/map/5g

TABLE I
gNB AND aUE PARAMETERS

Parameter	Value
Carrier frequency f_c	780 MHz
gNB	
Transmit power $P_{\text{T,gNB}}$	46 dBm
Mast height h_{gNB}	35 m
Sector antenna directions	30°, 150°, 270° in azimuth angles
Mechanical down-tilt	3°
Sector antenna model	8×1 ULA with element spacing of 0.5λ
aUE	
Height h_{UE}	variable
Antenna model	$\sqrt{N_{\text{e}}} \times \sqrt{N_{\text{e}}}$ uniform rectangular array with variable size and 0.5λ element spacing

where $P_{\text{T,dBm}}$ is the gNB transmit power in dBm, $G_{\text{T,dBi}}$ and $G_{\text{R,dBi}}$ are the antenna gains at the gNB and the aUE, respectively, in dBi while L_{dB} is the path loss in dB.

1) Link Quality: In interference-dominant environments, the SIR can be used for rating the link quality. The average SIR in dB is given by

$$\gamma = \bar{P}_{\text{S,dBm}} - \bar{P}_{\text{I,dBm}}, \tag{2}$$

where $\bar{P}_{\text{S}}{=}10^{\bar{P}_{\text{S,dBm}}/10}$ is the average power of the serving cell signal in mW and $\bar{P}_{\text{I}}{=}10^{\bar{P}_{\text{I,dBm}}/10}$ is the average interference power in mW.

Let N_{gNB} be the cardinality of the set $\mathcal{G}{=}\mathcal{G}_{\text{Sw}}{\cup}\mathcal{G}_{\text{Fo}}$. Then, the average power received from any gNB sector can be denoted as $\bar{P}_{\text{R}}^{g,s}$, where $g{\in}\mathcal{G}{=}\{1,\ldots,N_{\text{gNB}}\}$ identifies the gNB and $s \in \mathcal{S} = \{1,2,3\}$ identifies its sector. The interference power $\bar{P}_{\text{I}}$ in (2) is computed as the sum of received powers from all sectors in the network except the sectors of the serving gNB. If the gNB g' serves the aUE via its sector s', then $\bar{P}_{\text{S}} = \bar{P}_{\text{R}}^{g',s'}$ and

$$\bar{P}_{\text{I}} = \sum_{\tilde{g}\in\mathcal{G}\setminus g'} \sum_{\tilde{s}\in s} \bar{P}_{\text{R}}^{\tilde{g},\tilde{s}}. \tag{3}$$

2) Outage Probability: The outage probability p_{out} is defined as the probability of the instantaneous SIR falling below a threshold value γ_{min}. The instantaneous SIR can be obtained from the instantaneous received power $P_{\text{R,dBm}}^{g,s}$ given by:

$$P_{\text{R,dBm}}^{g,s} = \bar{P}_{\text{R,dBm}}^{g,s} + X_{\text{dB}}^{g,s}, \tag{4}$$

where $\bar{P}_{\text{R,dBm}}^{g,s}$ is computed according to (1) and $X_{\text{dB}}^{g,s}$ is a random variable distributed according to $\mathcal{N}(0,\sigma_X^{g,s})$ that captures shadow fading. The notation $\mathcal{N}(\mu,\sigma)$ denotes a Gaussian distribution with mean μ in dB and standard deviation σ in dB. Thus, the received power level of the serving gNB and of each interfering gNB are distributed according to $\mathcal{N}\left(\bar{P}_{\text{R,dBm}}^{g,s}, \sigma_{X,}^{g,s}\right)$.

The probability density function of the total instantaneous interference power $P_{\text{I,dBm}}$ is obtained using the Fenton-Wilkinson approximation [22] so that it is distributed according to $\mathcal{N}(\bar{P}_{\text{I,dBm}}^{\text{FW}}, \sigma_X^{\text{FW}})$. Here, $\bar{P}_{\text{I,dBm}}^{\text{FW}}$ and σ_X^{FW} are calculated from $P_{\text{R}}^{\tilde{g},\tilde{s}}$ and $\sigma_X^{\tilde{g},\tilde{s}}$ with $\tilde{g}{\in}\mathcal{G} \setminus g', \tilde{s}{\in}\mathcal{S}$ using the Fenton-Wilkinson method. Finally, with $\sigma_X^{\text{S}}{=}\sigma_X^{g',s'}$ the outage probability is given as:

$$p_{\text{out}} = \frac{1}{2}\text{erfc}\left(\frac{\gamma_{\text{FW}} - \gamma_{\text{min}}}{\sqrt{2}\sigma_{\text{SIR}}}\right), \tag{5}$$

where erfc() is the complementary error function, $\gamma_{\text{FW}} = \bar{P}_{\text{S,dBm}}{-}\bar{P}_{\text{I,dBm}}^{\text{FW}}$ and $\sigma_{\text{SIR}}{=}\sqrt{(\sigma_X^{\text{S}})^2 + (\sigma_X^{\text{FW}})^2}$ are the mean SIR and its standard deviation, respectively, according to the Fenton-Wilkinson approximation.

3) Availability: The availability is defined as the ratio, in percentage, of the time period in which the end-to-end communication service is delivered with an agreed Quality of Service (QoS) to the total period of time in which the system is expected to deliver the end-to-end service [23]. In this study, the availability is determined for the downlink quality by using the outage probability as measure of agreed QoS with respect to the minimum SIR threshold γ_{min}. Hence, the availability is given by the duration for which the p_{out} is below a threshold $p_{\text{out}}^{\text{th}}$, divided by the total duration of the approach trajectory.

D. Channel

The ATG channel model used for evaluating the link budget is altitude dependent and constructed from existing 3rd Generation Partnership Project (3GPP) channel models as follows:

For aUE altitudes $h_{\text{UE}} \leq 300\,\text{m}$, the channel model of a rural macro scenario for UAVs is adopted from [2]. The model from [12] is used for $h_{\text{UE}} > 300\,\text{m}$. The threshold altitude is chosen because the UAV channel model is valid for $h_{\text{UE}} \leq 300\,\text{m}$ [2].

A probabilistic path loss is used as in [24];

$$L_{\text{dB}} = p_{\text{LOS}} L_{\text{LOS}} + (1 - p_{\text{LOS}}) L_{\text{NLOS}}, \tag{6}$$

where L_{LOS} and L_{NLOS} are the path loss values in Line of Sight (LOS) and Non Line of Sight (NLOS) conditions, respectively, while p_{LOS} denotes the probability of LOS conditions. A similar approach is used for computing the average shadow fading standard deviation σ_X:

$$\sigma_X = p_{\text{LOS}}\sigma_{X,\text{LOS}} + (1 - p_{\text{LOS}})\sigma_{X,\text{NLOS}}, \tag{7}$$

where $\sigma_{X,\text{LOS}}$ and $\sigma_{X,\text{NLOS}}$ are the standard deviations of the shadow fading in LOS and NLOS conditions, respectively.

The path loss and shadow fading models adopted from [2] for $h_{\text{UE}} \leq 300\,\text{m}$ are given in Table II. The values of p_{LOS} are taken from Table B-1 of [2] which saturate to 1 at $h_{\text{UE}}{=}40\,\text{m}$. For $h_{\text{UE}}{>}300\,\text{m}$, free space propagation in LOS conditions is assumed [12]. The standard deviation $\sigma_{X,\text{LOS}}$ is obtained by linear interpolation from Table III.

TABLE II
CHANNEL MODEL FOR $h_{\text{UE}} \leq 300\,\text{m}$

Parameter	Model
L_{LOS}	$\max(23.9 - 1.8\log_{10}(h_{\text{UE}}), 20)\log_{10}(d)$ $+20\log_{10}(\frac{40\pi f_c}{3})$
L_{NLOS}	$\max(L_{\text{LOS}}, -12 + (35 - 5.3\log_{10}(h_{\text{UE}}))$ $\log_{10}(d) + 20\log_{10}(\frac{40\pi f_c}{3}))$
$\sigma_{X,\text{LOS}}$	$4.2\exp(-0.0046 h_{\text{UE}})$
$\sigma_{X,\text{NLOS}}$	6.0

TABLE III
$\sigma_{X,\mathrm{LOS}}$ FOR $h_{\mathrm{UE}} > 300\,\mathrm{m}$ AND ELEVATION ANGLES θ

θ	10°	20°	30°	40°	50°	60°	70°	80°	90°
$\sigma_{X,\mathrm{LOS}}$	1.79	1.14	1.14	0.92	1.42	0.56	0.85	0.72	0.72

E. Handovers

As the aUE moves over the TMCN, the serving gNB may need to be changed via handover procedure to ensure a sufficient link quality. In this work, the handover procedure is modeled as follows:

First: At any point on the trajectory, the receive signal power levels of all gNBs in radio range are obtained from one antenna element of the AESA. Thus, the $\bar{P}_{\mathrm{R}}^{\tilde{g},\tilde{s}}$ values are subject to the directivity of the antenna elements only.

Second: From the set of gNBs whose power levels were obtained, a subset $\mathcal{G}_{\mathrm{H}}$ containing $|\mathcal{G}_{\mathrm{H}}|$=64 gNBs with the strongest power levels is created. For each gNB in $\mathcal{G}_{\mathrm{H}}$, the $\bar{P}_{\mathrm{R}}^{\tilde{g},\tilde{s}}$ values are calculated assuming the AESA to be configured such that its main beam is directed towards the gNB. Using these values, the SIR is computed with the gNB signal as wanted component and the sum of the signals of all other gNBs as interference component. The gNB in $\mathcal{G}_{\mathrm{H}}$ with the highest SIR is selected as a handover candidate for the particular trajectory point. The rather large set size was chosen to make sure that the cells offering high SIR remain in the set $\mathcal{G}_{\mathrm{H}}$.

Third: A handover is performed, if the SIR from the handover candidate exceeds the SIR from the serving gNB by more than 3 dB. The procedure is constrained by a minimum time interval of 1 s between subsequent handovers.

III. Evaluation

The ATG link quality is evaluated on three flight trajectories, where aircraft approach one of the three runways of the Zurich airport. The trajectories are based on real data obtained from Flightradar24.com for flights departing from Rome, Venice and Philadelphia. The approach segments of these trajectories are depicted in Fig. 2. The evaluation considers scenarios with different levels of support provided by the TMCN. Recall that g' and $\tilde{g}$ denote the serving and interfering gNB, respectively, while $\mathcal{G}$=$\mathcal{G}_{\mathrm{Sw}}\cup\mathcal{G}_{\mathrm{Fo}}$. The scenarios are as follows:

A. No Support

The no-support scenario is the baseline case where the aUE is treated as normal terrestrial UE. Hence, $g'\in\mathcal{G}_{\mathrm{Sw}}$ and $\tilde{g}\in\mathcal{G}\setminus g'$.

B. Roaming Support

In the roaming-support scenario, the foreign network is not merely a source of interference but can also provide a serving gNB to the aUE. In this case, $g'\in\mathcal{G}$ while $\tilde{g}\in\mathcal{G}\setminus g'$. Roaming support can be beneficial at airports which are close to international borders such as the Zurich airport. It is acknowledged that cross border handovers are more complicated than intra-operator handovers [25]. However, the two classes of handovers are performed identically in this work.

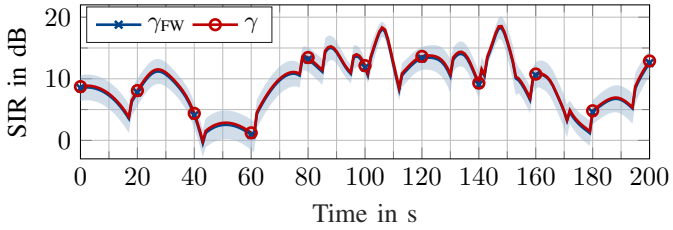

Fig. 3. SIR with a 8×8 AESA along the Rome trajectory.

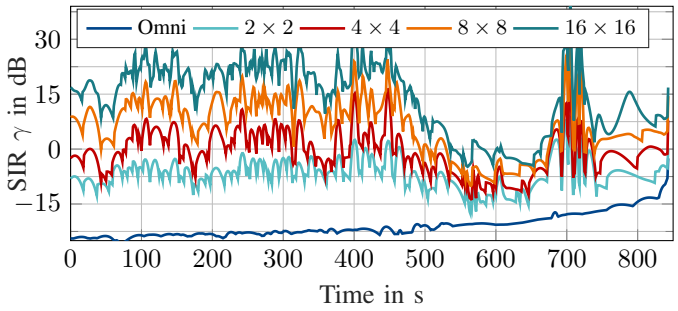

Fig. 4. SIR along the Rome trajectory for various antenna arrays at the aUE

C. Scheduling Support

In the scheduling-support scenario, the network supports the aUEs in terms of dedicated time-frequency resources. The resources allocated to the aUE are orthogonal to those allocated to the terrestrial UEs. Thus, traffic generated by terrestrial UEs does not cause interference at the aUE.

The allocation of dedicated resources can be realized in the form of a network slice. In our model, a network slice is assumed to be provided by a set of gNBs $\mathcal{G}^r_{\mathrm{Slice}} \subseteq \mathcal{G}_{\mathrm{Sw}}$. The set $\mathcal{G}^r_{\mathrm{Slice}}$ contains all the gNBs that fall within r=50 km of the Zurich airport. In this scenario, the serving gNB can only be among the gNBs hosting the slice, hence $g' \in \mathcal{G}^r_{\mathrm{Slice}}$. Hence, an interfering gNB will belong to the set $\tilde{g} \in (\mathcal{G}_{\mathrm{Sw}} \setminus \mathcal{G}^r_{\mathrm{Slice}}) \cup \mathcal{G}_{\mathrm{Fo}}$.

IV. Results and Discussion

Results are presented for the ATG link quality in terms of average SIR and availability, and handover behavior observed for the three trajectories. Fig. 3 depicts an example of the average SIR γ according to (2) as well as its approximation γ_{FW}. The figure also includes the $\pm 2\sigma_{\mathrm{SIR}}$ envelope (shaded regions) for γ_{FW}. Fig. 3 shows that depending upon the σ_{SIR} the average SIR needs to be sufficiently higher than γ_{min} for avoiding communications outages. Further, it can be seen that γ_{FW} underestimates the computed SIR γ only slightly.

A. Link quality

The link quality is evaluated with respect to the AESA configurations listed in Table IV and level of support by the TMCN in the following.

1) No Support: Fig. 4 shows the average SIR along the Rome to Zurich trajectory for the different AESA configurations.The figure also includes the SIR using an omnidirectional antenna at the aUE as a reference. The SIR observed in omnidirectional setup highlights the severity of interference at high altitudes. However, the AESA improves the SIR significantly where arrays with N_{e}=4, 16, 64 and 256 elements

TABLE IV
AIRCRAFT AESA CONFIGURATION WITH $\lambda = 0.38\,\text{m}$

Array configuration	2×2	4×4	8×8	16×16
No. of Elements N_e	4	16	64	256
Physical dimension in m^2	$(0.19)^2$	$(0.58)^2$	$(1.34)^2$	$(2.88)^2$

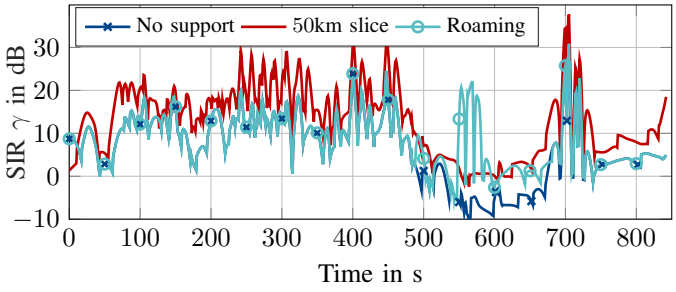

Fig. 5. SIR for the Rome trajectory with a 8×8 AESA.

increase the SIR by $14.1, 20.2, 27.6$ and $35.2\,\text{dB}$ in average as compared to the omnidirectional antenna.

The SIR curves in Fig. 4 exhibit a visible dip between the 500 and $700\,\text{s}$ marks that is independent from the AESA configuration. This is due to the fact that this portion of the trajectory is close to and even partially across the Swiss-German border where the Swiss network has poor coverage.

The physical dimension along each side of the AESA configurations in Table IV is estimated using the relation $0.5\lambda(\sqrt{N_e}-1)$. Assuming that the physical size of the 16×16 array is too large to be feasible, the 8×8 antenna array is chosen for the rest of evaluations. The average SIR observed along the Rome, Venice and Philadelphia is shown in Figs. 5, 6 and 7, respectively, with respect to the different levels of support by the TMCN. Without support by the network, negative SIR values can be observed in each trajectory.

2) Roaming & Scheduling Support: For the Rome trajectory, Fig. 5 shows that roaming support improves the SIR by up

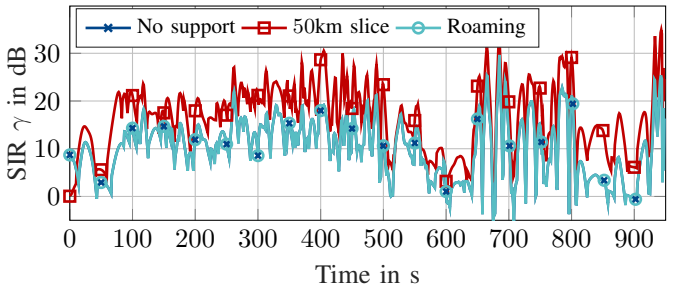

Fig. 6. SIR for the Venice trajectory with a 8×8 AESA.

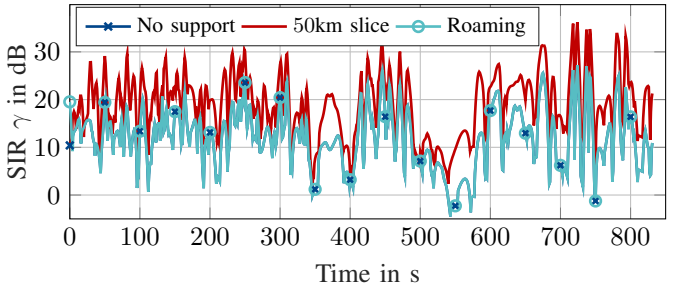

Fig. 7. SIR for the Philadelphia trajectory with a 8×8 AESA.

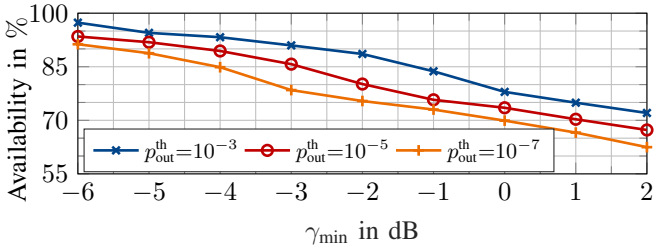

Fig. 8. Availability with different values for γ_{min} and $p_{\text{out}}^{\text{th}}$ for the Venice trajectory using 8×8 AESA in no support scenario.

TABLE V
AVAILABILITY IN % FOR $p_{\text{out}}^{\text{th}} = 10^{-5}$ W.R.T. $\gamma_{\text{min}} = 0$ (AND -6 dB)

Scenario	Rome	Venice	Philadelphia
No support	55.5 (78.6)	73.5 (93.5)	81.3 (97.5)
Roaming	59.9 (86.1)	73.5 (93.5)	81.3 (97.5)
Scheduling	71.7 (91.7)	92.1 (100)	97.7 (100)

to $30\,\text{dB}$. This improvement is, however, limited to the portion of the trajectory near the border. Support by network slicing increases the SIR on average by $6.5\,\text{dB}$ along the complete trajectory with up to $14\,\text{dB}$ improvement at the $337\,\text{s}$ mark.

Fig. 6 shows an average improvement of $6.29\,\text{dB}$ from the scheduling support for the Venice trajectory with up to $16\,\text{dB}$ increase at the $436\,\text{s}$ mark. The roaming support does not affect the SIR since the trajectory is far away from the border.

For the Philadelphia trajectory, Fig. 7 shows that the scheduling support improves the SIR by up to $14.4\,\text{dB}$ (at $124\,\text{s}$ mark) with an average SIR improvement of approx. $7\,\text{dB}$. Only marginal improvements of the SIR can be observed in case of support by roaming.

3) Availability: Fig. 8 shows the link availability for multiple $p_{\text{out}}^{\text{th}}$ w.r.t. a range of γ_{min}. It can be seen that stringent QoS requirements, i.e., low $p_{\text{out}}^{\text{th}}$ w.r.t. a high γ_{min}, lead to low availability and vice versa. Table V presents the availability of the ATG link if $p_{\text{out}}^{\text{th}}{=}10^{-5}$ is assumed together with a rather strict minimum SIR requirement of $\gamma_{\text{min}}{=}0\,\text{dB}$. For reference, the table also includes availability computed with $\gamma_{\text{min}}{=}{-6}\,\text{dB}$ [2]. Without support by the TMCN, the aerial link is available 55.5, 73.5 and 81.3 percent of the time for the Rome, Venice and Philadelphia trajectory, respectively. Roaming support slightly increases the availability only for the Rome trajectory. Support by scheduling significantly increases the link availability to 71.7, 92.1 and 97.7 percent of the time for the Rome, Venice and Philadelphia trajectory, respectively.

B. Handovers

Table VI contains handover data for the flight trajectories in the three evaluation scenarios. The table provides the mean of the time intervals between handovers $\bar{T}_{\text{HO}}$ and the largest interval between consecutive handovers T_{max} in seconds. The smallest inter-handover interval across all the scenarios was observed to be $1\,\text{s}$.

For each scenario, the corresponding row in Table VI shows that the handover frequency increases from left to right. For instance, the trajectories from Rome, Venice and Philadelphia require on average a handover every $12.23, 11.42$ and $8.65\,\text{s}$,

TABLE VI
HANDOVER INTERVALS IN SECONDS IN VARIOUS SCENARIOS

	Rome		Venice		Philadelphia	
Scenario	$\bar{T}_{\text{HO}}$	$T_{\max}$	$\bar{T}_{\text{HO}}$	$T_{\max}$	$\bar{T}_{\text{HO}}$	$T_{\max}$
No support	12.23	67	11.42	45	8.65	37
Roaming	11.53	67	11.42	45	8.56	37
Scheduling	11.4	44	10.42	42	7.82	35

respectively, in the baseline scenario. Together with Table V, the handover data reveals that high availability comes with more frequent handovers. The same trend is seen by considering columns of the same trajectory in the two tables. Recall (cf. Sec II-E) that handovers are executed whenever a candidate gNB is better by 3 dB from the serving one regardless of the case that the SIR from the serving gNB might be above the γ_{min}. This, combined with the aUE traversing the sidelobes of the gNB's antenna gain pattern leads to the direct relation between the availability and handover frequency.

V. CONCLUSION

This work evaluated the feasibility of using ATG communications to support the safe landing of a passenger aircraft in approach to an airport by means of a remote operator. The focus was on the interference affected downlink established with a 5G network that is optimized for terrestrial coverage. The results were obtained using link budget simulations yielding SIR and availability values for real approach trajectories. It is shown that an acceptable level in SIR can be achieved with an 8×8 AESA installed onboard the aircraft, providing up to 81.3% availability.

The presented results demonstrate that significant improvements in SIR and availability can be achieved when the TMCNs supports ATG communications by provisioning dedicated resources, e.g., in form of a network slice. With the dedicated resources, a downlink availability of up to 97.7% was achieved. Depending upon proximity of international borders, roaming support might be crucial. Further, this work indicated a direct relation between handover frequency and link availability.

Finally, it is pointed out that this work assumed the gNBs to be equipped with down-tilted antennas. Measures to support aerial users in TMCN, such as up-tilted antennas and electrical beam steering at the gNBs together with favorable gNB locations are expected to drastically improve link quality and reduce the handover frequency in ATG communications. Moreover, carrier frequencies higher than 780 MHz, as considered in [12], can enable the use of AESAs larger than 8×8 which can also be helpful. With these measures, a link availability approaching 100% can be expected.

REFERENCES

[1] RTCA, *Minimum Aviation System Performance Standards for C2 Link Systems Supporting Operations of Unmanned Aircraft Systems in U.S. Airspace*, Radio Technical Commission for Aeronautics Std. DO-377, Mar. 2019.

[2] 3GPP, "Enhanced LTE support for aerial vehicles," 3rd Generation Partnership Project, TR 36.777, 01 2018, ver. 15.0.0.

[3] I. Kovacs, R. Amorim, H. C. Nguyen, J. Wigard, and P. Mogensen, "Interference Analysis for UAV Connectivity over LTE Using Aerial Radio Measurements," in *2017 IEEE 86th Vehicular Technology Conference (VTC-Fall)*, 2017, pp. 1–6.

[4] X. Lin, V. Yajnanarayana, S. D. Muruganathan, S. Gao, H. Asplund, H.-L. Maattanen, M. Bergstrom, S. Euler, and Y.-P. E. Wang, "The Sky Is Not the Limit: LTE for Unmanned Aerial Vehicles," *IEEE Communications Magazine*, vol. 56, no. 4, pp. 204–210, 2018.

[5] S. D. Muruganathan, X. Lin, H.-L. Määttänen, J. Sedin, Z. Zou, W. A. Hapsari, and S. Yasukawa, "An Overview of 3GPP Release-15 Study on Enhanced LTE Support for Connected Drones," *IEEE Communications Standards Magazine*, vol. 5, no. 4, pp. 140–146, 2021.

[6] Qualcomm, "LTE Unmanned Aircraft Systems," Qualcomm Technologies, Inc, Trail Report 38.811, 5 2017, version 1.0.1.

[7] Y. Zeng, Q. Wu, and R. Zhang, "Accessing From the Sky: A Tutorial on UAV Communications for 5G and Beyond," *Proceedings of the IEEE*, vol. 107, no. 12, pp. 2327–2375, 2019.

[8] R. Muzaffar, C. Raffelsberger, A. Fakhreddine, J. L. Luque, D. Emini, and C. Bettstetter, "First Experiments with a 5G-Connected Drone," in *6th ACM Workshop on Micro Aerial Vehicle Networks, Systems, and Applications*, ser. DroNet '20. New York, USA: Association for Computing Machinery, 2020.

[9] V. Marojevic, I. Guvenc, R. Dutta, M. L. Sichitiu, and B. A. Floyd, "Advanced Wireless for Unmanned Aerial Systems: 5G Standardization, Research Challenges, and AERPAW Architecture," *IEEE Vehicular Technology Magazine*, vol. 15, no. 2, pp. 22–30, 2020.

[10] 3GPP, "5G; Unmanned Aerial System (UAS) Support in 3GPP," 3rd Generation Partnership Project, TS 22.125, 04 2022, ver. 17.6.0.

[11] "European aviation network," https://www.europeanaviationnetwork.com, accessed: 2023-04-28.

[12] 3GPP, "Study on Air-to-ground network for NR," 3rd Generation Partnership Project, TR 38.876, 01 2022, ver. 16.16.0.

[13] V. Yajnanarayana, Y.-P. Eric Wang, S. Gao, S. Muruganathan, and X. Lin Ericsson, "Interference Mitigation Methods for Unmanned Aerial Vehicles Served by Cellular Networks," in *2018 IEEE 5G World Forum (5GWF)*, 2018, pp. 118–122.

[14] H. C. Nguyen, R. Amorim, J. Wigard, I. Z. KováCs, T. B. Sørensen, and P. E. Mogensen, "How to Ensure Reliable Connectivity for Aerial Vehicles Over Cellular Networks," *IEEE Access*, vol. 6, pp. 12 304–12 317, 2018.

[15] T. Izydorczyk, M. Bucur, F. M. L. Tavares, G. Berardinelli, and P. Mogensen, "Experimental Evaluation of Multi-Antenna Receivers for UAV Communication in Live LTE Networks," in *2018 IEEE Globecom Workshops (GC Wkshps)*, 2018, pp. 1–6.

[16] Y. Huang, Q. Wu, T. Wang, G. Zhou, and R. Zhang, "3D Beam Tracking for Cellular-Connected UAV," *IEEE Wireless Communications Letters*, vol. 9, no. 5, pp. 736–740, 2020.

[17] T. Izydorczyk, G. Berardinelli, P. Mogensen, M. M. Ginard, J. Wigard, and I. Z. Kovács, "Achieving High UAV Uplink Throughput by Using Beamforming on Board," *IEEE Access*, vol. 8, pp. 82 528–82 538, 2020.

[18] A. Colpaert, E. Vinogradov, and S. Pollin, "3D beamforming and handover analysis for UAV networks," in *2020 IEEE Globecom Workshops*, 2020, pp. 1–6.

[19] Swiss Federal Office of Communications, "Location of radio transmitters," accessed 30 March 2022. [Online]. Available: https://www.bakom.admin.ch/bakom/en/homepage/frequencies-and-antennas/location-of-radio-transmitters.html

[20] 3GPP, "5G; Study on channel model for frequencies from 0.5 to 100 GHz," 3rd Generation Partnership Project, TR 38.901, 11 2020, ver. 16.1.0.

[21] ITU-R, "Characteristics of terrestrial IMT-Advanced systems for frequency sharing/interference analyses," International Telecommunication Union, Tech. Rep. M.2292-0, Dec. 2013.

[22] G. L. Stüber, *Principles of Mobile Communication*, 4th ed. Springer-Verlag GmbH, 2017.

[23] 3GPP, "5G; Service requirements for the 5G system," 3rd Generation Partnership Project, TS 22.261, 01 2022, ver. 16.16.0.

[24] W. Shin and M. Vaezi, "UAV-Enabled Cellular Networks," in *5G and Beyond*. Springer, 2021, pp. 165–200.

[25] A. Kousaridas, M. Fallgren, E. Fischer, F. Moscatelli, R. Vilalta, M. Mühleisen, S. Barmpounakis, X. Vilajosana, S. Euler, B. Tossou, and J. Alonso-Zarate, "5G Vehicle-to-Everything Services in Cross-Border Environments: Standardization and Challenges," *IEEE Communications Standards Magazine*, vol. 5, no. 1, pp. 22–30, 2021.